Revealing the Substrate Constraint Effect on the Thermodynamic Behaviour of the Pd–H through Capacitive-Based Hydrogen-Sorption Measurement

Gwangmook Kim, Soomin Lee, Sang-kil Lee, Han Jun Yu, Hunyoung Cho, Youngjun Chung, Tae-Eon Park, Hyun-Sook Lee, Wooyoung Shim, Kyu Hyoung Lee, Jeong Young Park, Yu Jin Kim,* Dong Won Chun,* and Wooyoung Lee*

Mechanical constraints imposed on the Pd–H system can induce significant strain upon hydrogenation-induced expansion, potentially leading to changes in the thermodynamic behavior, such as the phase-transition pressure. However, the investigation of the constraint effect is often tricky due to the lack of simple experimental techniques for measuring hydrogenation-induced expansion. In this study, a capacitive-based measurement system is developed to monitor hydrogenation-induced areal expansion, which allows us to control and evaluate the magnitude of the substrate constraint. By using the measurement technique, the influence of substrate constraint intensity on the thermodynamic behavior of the Pd–H system is investigated. Through experiments with different constraint intensities, it is found that the difference in the constraint intensity minimally affects the phase-transition pressure when the Pd–H system allows the release of constraint stress through plastic deformation. These experiments can improve the understanding of the substrate constraint behaviours of Pd–H systems allowing plastic deformation while demonstrating the potential of capacitive-based measurement systems to study the mechanical–thermodynamic coupling of M–H systems.

1. Introduction

The ever-increasing demand for renewable energy has promoted extensive research into alternatives to fossil fuels. As such, hydrogen is being widely explored as a promising substitute for fossil fuels in light of its numerous advantages, namely, its high energy density, abundance on Earth and low environmental impact upon combustion.[1] However, the utilization of metal hydrides as hydrogen storage systems faces significant challenges due to thermodynamic and kinetic limitations, hindering their widespread adoption.[2]

In this context, significant efforts have been dedicated to engineering the thermodynamics and hydrogen absorption/desorption kinetics of metal hydrides, for example, through size reduction,[3–5] catalysis[6–8] and alloying.[9–11] Notably, manipulation of the mechanical stress provides an efficient engineering strategy for tuning the thermodynamics and kinetics of metal hydrides while maintaining their chemical composition and morphology. During the hydrogenation process, which is accompanied by volume expansion, a metal hydride experiences substantial mechanical stress. This mechanical stress can induce elastic strain energy and plastic deformation in the metal hydride, leading to a shift in the phase-transition pressure[12,13] and irreversibility in the hydrogen ab/desorption cycle.[14] The deformation behavior is affected by the internal

G. Kim, S. Lee, S.-kil Lee, Y. Chung, H.-S. Lee, W. Shim, K. H. Lee, Y. J. Kim, D. W. Chun, W. Lee
Department of Materials Science and Engineering
Yonsei University
Seoul 120–749, South Korea
E-mail: yujin.kim@yonsei.ac.kr; chundream98@kist.re.kr; wooyoung@yonsei.ac.kr
G. Kim, Y. J. Kim
KIURI Institute
Yonsei University
Seoul 03722, Republic of Korea

H. J. Yu, H. Cho, D. W. Chun
Center for Energy Materials Research
Korea Institute of Science and Technology (KIST)
Seoul 02792, Republic of Korea
J. Y. Park
Department of Chemistry
Korea Advanced Institute of Science and Technology (KAIST)
Daejeon 34141, South Korea
T.-E. Park
Center for Spintronics
Korea Institute of Science and Technology (KIST)
Seoul 02792, South Korea
D. W. Chun
Yonsei-KIST Convergence Research Institute
Yonsei University
Seoul 03722, Republic of Korea

ADVANCED
SCIENCE NEWS
www.advancedsciencenews.com

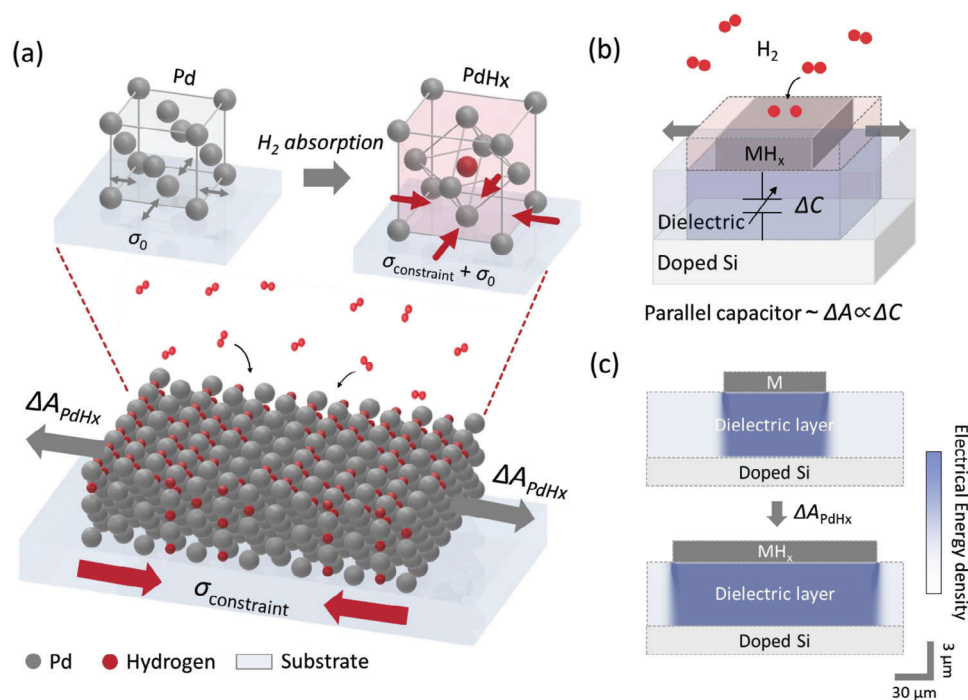ADVANCED
MATERIALS
www.advmat.de

Figure 1. Experimental principles. a) Illustration depicting the substrate constraint effect on hydrogenation-induced expansion of the host metal. b) Principle of the capacitance measurement to measure the change in the interfacial area between metal hydride and the dielectric layer/doped Si substrate upon hydrogenation. c) Simulation results of the electrical energy density in the metal hydride/dielectric layer/doped Si substrate.

deformation mechanism[15–18] and external constraints.[12–14,19,20] For example, nanosized Pd shows a different plateau pressure from bulk Pd due to the elastic constraints induced by the internal hydrogenation mechanism.[17,18] Hydrogenation-induced stress on LaNi$_5$ introduces dislocations and cracks, which decrease the plateau pressure in the following absorption cycle.[21] The Mg–H system can be destabilized by elastic clamping using a Pd capping layer.[13,14,22] The constrained Mg–H system can stabilize metastable γ-MgH$_2$.[23] The results of a study on an Nb–H system adhered to a substrate show that the yield stress determines the critical hydrogen concentration affecting the elastic and plastic behaviours.[24] These behaviours can be modified by changing the thickness of the metal film.[25] The microstructural factors of the Pd film affect the hydrogenation behaviours under clamping conditions.[20] These effects are practically important for tuning the thermodynamics of hydrogen absorption/desorption in metal hydrides and enhancing their applications.

Despite the significant effect of mechanical stress on the thermodynamics of metal hydrides, its quantitative effect and underlying mechanism are challenging to investigate using conventional pressure–concentration isotherms. Since the influence of mechanical stress is closely tied to the dimensional changes of the host metal, in situ microscopy techniques[17,18] and X-ray diffraction[12,26] should be employed to observe the structural variation during hydrogenation. However, these techniques can be cumbersome and often offer limited investigation into the microstructural behavior, focusing primarily on the local

changes in certain spots rather than on the overall dimensional changes in the host metal. In particular, the aforementioned limitation makes it difficult to estimate the strain constraint ratio from the external constraints and the plastic deformation across the entire specimen.

In this study, we propose a novel capacitive-based measurement system designed to observe the dimensional changes of a metal film during the hydrogenation/dehydrogenation processes. Using our system, we investigate the influence of substrate constraint on the thermodynamics of the palladium hydride, which serves as a representative M–H system (**Figure 1a**). Our system enables high-resolution measurement of macroscopic areal expansion on the order of 0.01% by monitoring the capacitance change in a parallel structure that includes the host metal. Notably, this measurement can be achieved using simple electrical instruments. Substrate constraint effects, such as clamping at the interface, are recognized for their influence on the thermodynamics of metal hydrides through elastic strain energy.[13,20] Our novel system allows us to clearly reveal the effect of substrate constraint on the shift of the phase-transition pressure and the magnitude of plastic deformation by monitoring the constraint of hydrogen-induced areal expansion while controlling the strain constraint ratio at the interface. The results reveal the influence of constraint intensity on the thermodynamic behavior of a Pd–H system that allows plastic deformation while also demonstrating the potential of our experimental system for investigating M–H systems.

ADVANCED
SCIENCE NEWS
www.advancedsciencenews.com

ADVANCED
MATERIALS
www.advmat.de

2. Results and Discussion

2.1. Capacitive Measurement Of Hydrogenation-Induced Areal Expansion

We designed a capacitive-based measurement system by adopting a parallel structure of metal hydride (MHx)/dielectric layer/doped Si substrate (Figure 1b). During the experiments, the test unit was subjected to controlled hydrogen pressure in a sealed chamber, and we measured the capacitance change across the dielectric layer using an LCR meter (Figure S1, Supporting Information). The corresponding capacitance (C) of the parallel structure is described as follows:

$$C = \epsilon_0 \, \epsilon \, \frac{A_{Pd}}{t_{dielectric}} \tag{1}$$

where ϵ_0, ϵ and $t_{dielectric}$ are the vacuum permittivity, the relative permittivity of the dielectric layer and the thickness of the dielectric layer, respectively. By using the area–capacitance relationship in Equation (1), we can continuously monitor the hydrogenation-induced areal expansion ($\Delta A/A_0$) through the capacitance change ($\Delta C/C_0$), where ΔA represents the change in area and A_0 is the initial area. Figure 1c illustrates the working mechanism of our measurement system. The color gradient represents the electrical energy density derived by simulation, which reflects the amount of energy stored in the electric field of the parallel capacitor. As the MH$_x$ film expands, a wider electric field is induced in the out-of-plane direction, resulting in an increased amount of energy stored in the dielectric layer. This leads to an increase in capacitance as a response to the expanding area of the film.

From the mechanical perspective, the dielectric layer/doped Si substrate applies a mechanical constraint on the metal hydride film against hydrogenation-induced expansion. The strain transfer ratio from the Si substrate to the metal hydride can be controlled by adjusting the thickness of the interlayer and the area of the metal hydride film on the interlayer, as discussed in the following section.[27,28] This approach allows us to impose controlled mechanical stress on the metal hydride without changing the substrate materials. Notably, if the intensity of substrate constraint is controlled using different substrate materials, the interfacial alloying effect can blur the influence of mechanical constraint on the thermodynamic behaviour.[13,14,22] To investigate the substate constraint effect on the thermodynamics of the Pd–H system, we used polydimethylsiloxane (PDMS) as the dielectric interlayer due to its chemical inertness. The elastomeric behavior of PDMS ensures a wide range of tunability and consistency without experiencing mechanical failure at the interface, even during significant hydrogenation-induced expansion.[29,30] Since the hydrogen solubility of PDMS is very low,[31] PDMS can serve as a stable dielectric layer during hydrogen ab-/desorption experiments.

2.2. Effect of the Substrate Constraint on the Phase Transition from the α- to β-Phase

The substrate constraint on the Pd thin film is applied as a shear stress at the interface with the substrate (**Figure 2a**). In our test unit, the PDMS interlayer serves as a buffer to relieve the substrate constraint originating from the underlying silicon substrate. As a result, the effective constraint strain on the Pd film depends on the geometries of the PDMS and Pd layers. The relationship between the maximum strain of Pd (ϵ_{max}) and the geometric parameters can be described using the shear-lag model as follows[27,28] (Note S1, Supporting Information):

$$\frac{\epsilon_{max}}{\alpha_{Pd}} = 1 - \frac{1}{\cosh\sqrt{\frac{G_{PDMS} \cdot W^2}{4 E_{Pd} \cdot t_{PDMS} \cdot t_{Pd}}}} \tag{2}$$

where α_{Pd}, G_{PDMS}, E_{Pd}, W, t_{PDMS} and t_{Pd} are the linear expansion ratio of Pd, the shear modulus of PDMS, the Young's modulus of Pd, the width of the Pd pattern, the thickness of PDMS and the thickness of Pd, respectively. According to Equation (2), the intensity of the substrate constraint can be controlled by adjusting the width of the Pd film and the thicknesses of the Pd film and PDMS layer. The stable bonding interfaces between Pd and PDMS as well as between PDMS and Si are confirmed by the peel-off test (Figure S2, Supporting Information). While the thermodynamic and mechanical behaviours of a fully clamped Pd–H film by rigid substrate were investigated,[32] we designed this experiment to continuously control the intensity of the substrate constraint using Pd/PDMS/Si and thereby investigate the quantitative influence of constraint intensity. Some degree of hydrogenation-induced expansion is allowed depending on the constraint intensity. The amount of hydrogen-induced expansion is measured through a capacitive-based system to estimate the magnitude of substrate constraint strain.

In the experiments, we used a common 5 μm-thick PDMS layer and controlled the aspect ratio of the Pd patterns to manipulate the intensity of the constraint. The Pd patterns were designed in a serpentine shape to alleviate the accumulated strain in the longitudinal direction. Sputtered Pd films with various thicknesses were patterned into the desired widths using photolithography and a subsequent etching process (Figure 2b; Figure S3, Supporting Information). As the aspect ratio of the Pd patterns decreased, the constraint stress on the Pd film increased, as demonstrated by the finite element analysis results at a linear expansion of 3.5% (Figure 2c; Figure S4, Supporting Information). We used the same batch of sputtered Pd films to minimize the discrepancy in the initial thermal stress. The patterned Pd films exhibited similar X-ray diffraction (XRD) patterns in terms of the (111) and (200) peaks, for which the standard deviations of the 2θ peak position were 0.0497° and 0.0420°, respectively (Figure S5, Supporting Information). These results indicate that the patterned Pd films possess similar intrinsic stresses.

Figure 2d,e shows the capacitance changes of the test units with Pd patterns of different widths and thicknesses during the hydrogenation/dehydrogenation cycle, ranging from 0.2 to 4 kPa at 298 K (Figure S6, Supporting Information). All the test units exhibited a sudden increase and decrease in capacitance, indicating the area change at the phase transition of Pd from the α-phase to the β-phase. The in situ XRD pattern of the 50 nm Pd film on PDMS/Si was obtained while the system was under a hydrogen environment, showing a (111) peak shift from 40.17° to 38.76° at a hydrogen pressure of 4 kPa (Figure 2f). The corresponding lattice constant of hydrogenated Pd was 4.020 Å, which is consistent with that of β-phase Pd reported in a previous study (4.025 Å,
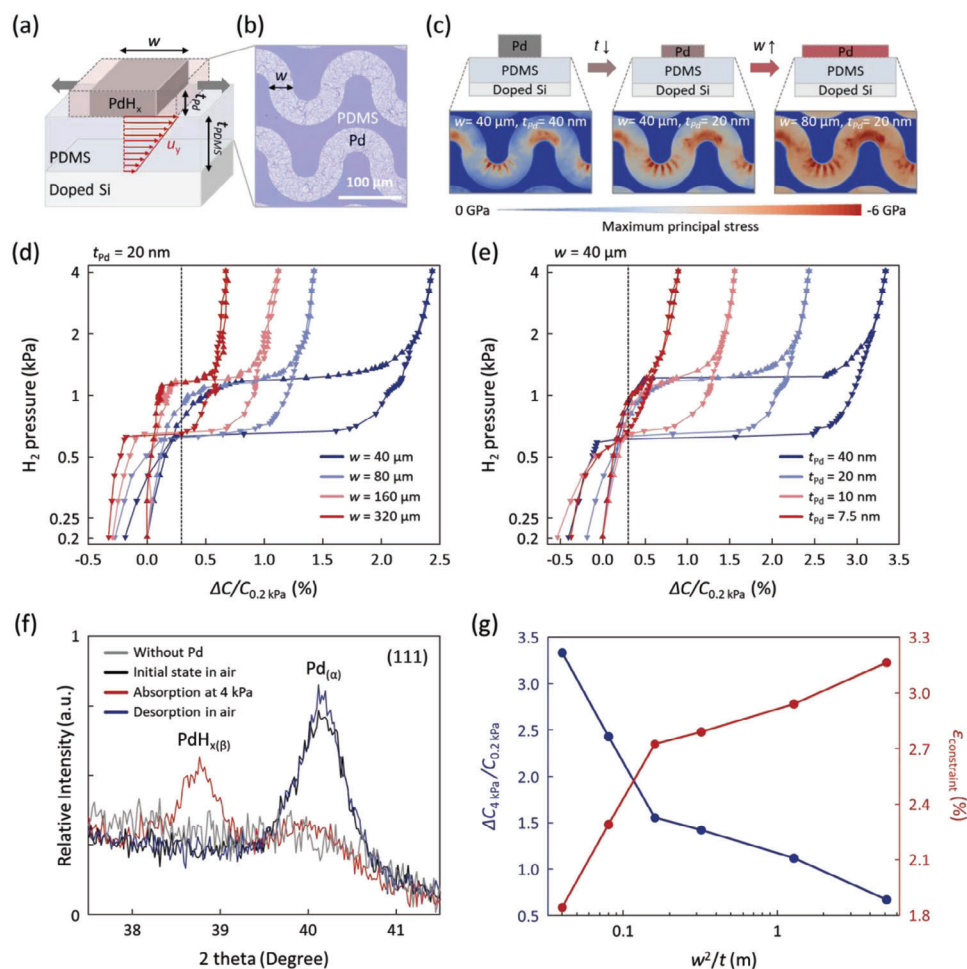
Figure 2. Constraint strain on the Pd–H system. a) Simplified model of displacement (u_y) in the Pd/PDMS/Si structure under hydrogenation-induced expansion of Pd. b) Optical microscopy image of the patterned Pd/PDMS/Si test unit. c) Simulation results of the elastic constraint stress for different thicknesses and patterned widths of Pd at a linear expansion of 3.5%. d,e) Capacitance change of test units during the hydrogen ab- (▲)/desorption (▼) cycle for different widths (d) and thicknesses (e) of Pd patterns. The reference for the relative capacitance change was the capacitance at 0.2 kPa. f) XRD patterns of the 50 nm-thick Pd film on the PDMS/Si substrate upon hydrogen ab/desorption. g) Maximum capacitance change (blue line) and corresponding constraint strain (red line) of the test units depending on the width and thickness of Pd patterns.

$PdH_{0.58 (\beta)}$[33]). Based on the XRD peak shift, the hydrogenation-induced lattice expansion was estimated to be 3.5%.

For the Pd patterns with different widths and thicknesses, the test units exhibited varying maximum capacitance (blue line in Figure 2g). We considered the maximum capacitance to correspond to the maximum areal expansion of each Pd pattern under the different constraint conditions ($C_{4 kPa} / C_{0.2 kPa} = A_{\beta}^{constrained} / A_{\alpha}$). By comparing the areal expansion with the lattice expansion ratio obtained from the XRD peak shift, we estimated the constraint strain on the Pd patterns ($\varepsilon_{constraint} = 103.5\% - \sqrt{C_{4 kPa}/C_{0.2 kPa}}$) (red line in Figure 2g), which indicated that wider and thinner Pd patterns resulted in a larger constraint strain, which aligns with the predictions of the shear-lag model.

Regarding the phase-transition behavior, all the Pd patterns exhibited similar plateau pressures in both hydrogen absorption and desorption despite the different magnitudes of the constraint

strain (**Figure 3a**). These plateau pressures deviated from the values predicted by the elastic constraint model, which considers the increase in the elastic contribution to the chemical potential of the expanded β-phase (Note S2, Supporting Information). Notably, the insensitivity of the plateau pressure was also observed in the Pd/SiO$_2$/Si test units (Figure S7, Supporting Information), where the substrate constraint was expected to be much higher than that in the Pd/PDMS/Si test units. The capacitance changes of the Pd/SiO$_2$/Si test units were noisier than those of the Pd/PDMS/Si test units due to the limited elastic behavior of SiO$_2$ and the small area change in the Pd patterns. The phase transition of Pd on SiO$_2$/Si was further confirmed by in situ XRD (Figure S8, Supporting Information). The hydrogenation-induced areal expansion of Pd patterns was almost fully clamped, on the order of 0.01%, which is consistent with the results of the in situ atomic force microscopy (AFM) measurements (Figure S9, Supporting Information). However, despite the
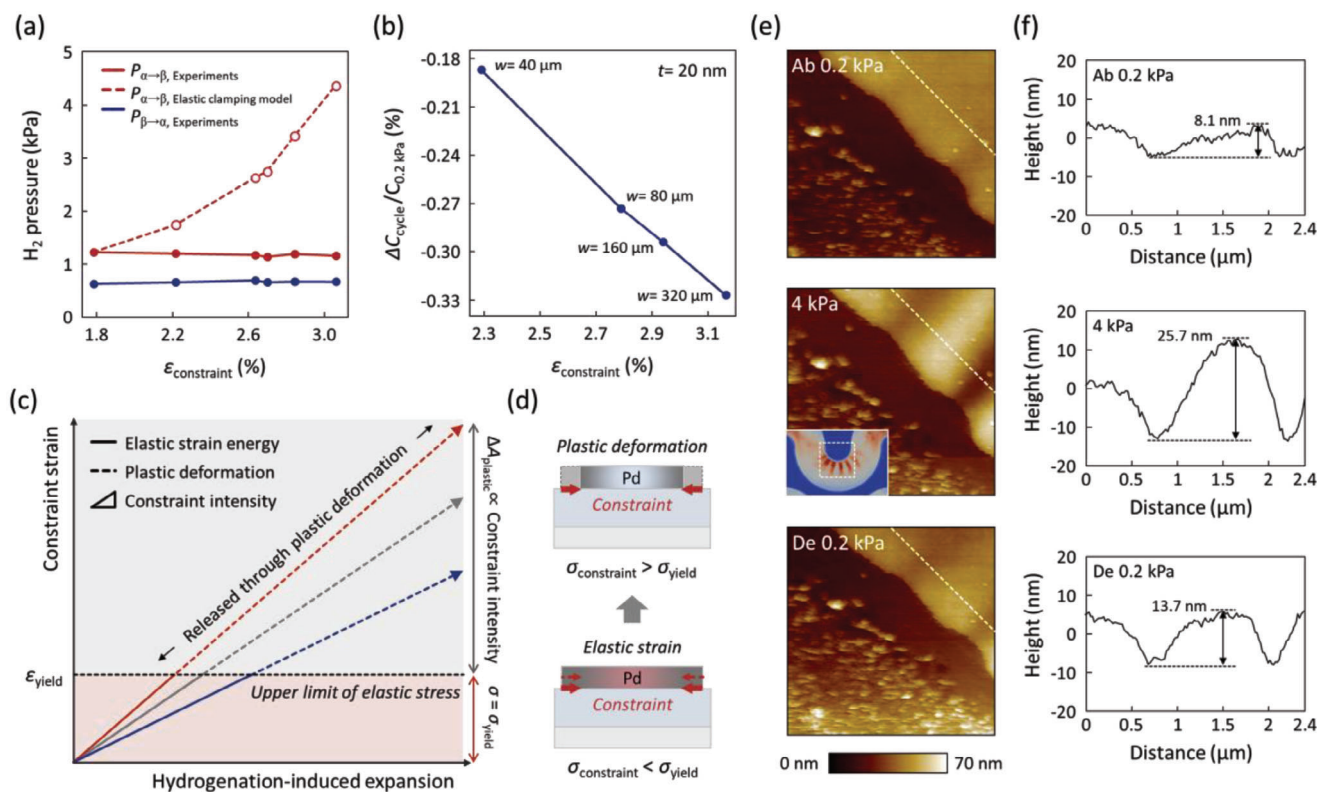
Figure 3. Constraint behavior of Pd patterns on PDMS/Si substrates. a) Plateau pressures of Pd patterns depending on the constraint strain. The plateau pressure was determined as the hydrogen pressure at the midpoint of the capacitance change. b) Areal shrinkage ratio of 20 nm-thick Pd patterns after the hydrogen ab/desorption cycle depending on the constraint strain. c) Schematic illustration of the thermally induced initial stress of the Pd film during the sputtering process onto the PDMS/Si substrate. d) Schematic graph describing the magnitude of the elastic strain and plastic deformation depending on the constraint intensity. d) Schematic illustrations of the deformation behavior of clamped Pd depending on the magnitude of the constraint stress. e) In situ AFM images of a Pd pattern with a width of 40 μm and a thickness of 20 nm on a PDMS/Si substrate. f) Line profiles of the Pd pattern during the hydrogen ab/desorption cycle along the broken lines in Figure 3e.

different levels of constraint strain, the phase-transition pressures remained in a similar range for the Pd patterns, from 1.6 to 1.8 kPa, which suggests that the elastic strain energy involved in the phase transition is constant regardless of the macroscopic constraint strain (Figure S7c, Supporting Information). If the increase in constraint strain does not contribute to the elastic strain energy, then the excess constraint strain may possibly be released through plastic deformation. For an M–H system adhered to a substrate, it has been reported that the hydrogenation-induced constraint stress over yield stress induces plastic deformation, thereby releasing the excess stress.[20,24] As evidenced by our experiments, we observe a decrease in the capacitance, indicating areal shrinkage of Pd, after the hydrogen absorption/desorption cycle relative to that in the initial state. This decrease can be attributed to atomic rearrangement along the out-of-plane direction during plastic deformation under the limited in-plane expansion. Interestingly, for the Pd patterns with identical thicknesses of 20 nm, the amount of shrinkage exhibited a linear increase with the constraint strain (Figure 3b). This suggests that the magnitude of plastic deformation is correlated with the intensity of the constraint, in contrast to the constant elastic strain observed in the plateau pressures.

The schematic graph in Figure 3c illustrates the proposed deformation behavior of clamped Pd during hydrogenation, which

helps explain the experimental results. Unless the plastic deformation of Pd films is suppressed, the constraint strain can result in both elastic compression and plastic deformation. The type of deformation depends on the magnitude of the constraint stress compared to the yield strength of Pd.

In the early stage of hydrogenation-induced expansion, the constraint strain can be stored as elastic strain energy, contributing to the chemical potential of Pd[20] (bottom of Figure 3d). Accumulation of elastic strain energy is reflected in an elevated plateau pressure,[20] in which the phase-transition pressure gradually increases due to the partial phase transition of the α-phase Pd. In our experiments, Pd patterns exhibited excess areal expansion beyond the upper limit of the α-phase (≈0.3%,[33] broken line in Figure 2d,e) before reaching the plateau pressure, which implies an elevated plateau pressure resulting from the partial phase transition in the early stage of hydrogenation. However, once the constraint stress exceeds the yield strength of Pd, the Pd patterns cannot accumulate the constraint stress as lattice strain. At this point, the excess constraint stress begins to be dissipated through plastic deformation (top of Figure 3d).

The substantial volume expansion that occurs during hydrogenation results in a constraint stress (e.g., $\sigma_{constraint} = \frac{E_{Pd}\varepsilon_{constraint}}{1-\nu_{Pd}} = 6.3$ GPa for $E_{Pd} = 110$ GPa, $\nu_{Pd} = 0.39$, and

ADVANCED
SCIENCE NEWS

www.advancedsciencenews.com

ADVANCED
MATERIALS

www.advmat.de

$\epsilon_{constraint}$ = 3.5%) that is generally much larger than the yield strength of Pd (≈ 1 GPa for a film under gas-phase loading conditions[34]). Therefore, plastic deformation is more likely to govern the overall deformation of clamped Pd during hydrogenation. Under this condition, the elastic contribution from the constraint stress to the chemical potential of Pd is limited to a constant value, namely, the yield strength of Pd, regardless of the constraint strain. The apparent macroscopic constraint strain only results from the increase in plastic deformation. Plastic deformation releases Pd films from their elastic constraints, regardless of the intensity of substrate constraint.

In situ AFM measurements were conducted to observe evidence of plastic deformation in the Pd patterns on PDMS/Si substrates (Figure 3e,f). Note that the plastic deformation of the thicknesses and areas of Pd patterns after the hydrogen ab-/desorption cycle should be on the order of 0.1%, which is usually difficult to track by AFM. We track the change in the surface morphology of the Pd film on PDMS after the hydrogen ab-/desorption cycle to observe the plastic deformation. In situ AFM measurements showed topographic images on the inner side of the serpentine patterns, where the hydrogenated Pd film experienced compressive stress from the substrate constraint (inset of Figure 3e). Initially, the Pd patterns exhibited a flat morphology (top of Figure 3e,f). However, upon hydrogenation, the expanded Pd underwent deformation and formed a wrinkled structure as a result of the compressive constraint stress from the PDMS/Si substrate (middle of Figure 3e,f). Due to the plastic behavior of Pd during constraint-induced deformation, the wrinkled morphology of the Pd pattern could not fully recover to the initial flat surface after dehydrogenation (bottom of Figure 3e,f).

The dissipation of the constraint strain through plastic deformation was also observed in the in situ AFM data of the Pd/SiO$_2$/Si test units (Figure S9, Supporting Information). While the areal expansion of the Pd pattern was fully clamped by the SiO$_2$/Si substrate, the hydrogenation-induced expansion of the thickness was $\Delta t_{4\,kPa}/t_{0.2\,kPa} \approx 9\%$ (Figure S9b, Supporting Information). This value is much higher than the expansion observed for the lattice constant ($\approx 3.5\%$). The excess expansion indicates severe plastic deformation in the out-of-plane direction resulting from the clamped areal expansion.[32] The elastic constraint strain of Pd can be dissipated through the plastic deformation while we didn't observe any delamination of the Pd pattern to be released from the substrate.

2.3. Comparing the Influences of Constraint Stress and Intrinsic Stress on the Plateau Pressure

Next, we conducted a comparison between constraint stress and intrinsic stress to investigate their influences on the hydrogenation process of Pd. As the degree of hydrogenation increases, the constraint stress gradually develops, while the intrinsic stress remains constant in magnitude from the initial state. By comparing the constraint and intrinsic stresses, we can gain insight into how the stresses influence changes in the hydrogen concentration and thereby elucidate the mechanism by which the constraint stress is involved in the hydrogenation reaction of Pd.

To quantitatively apply intrinsic stress on the Pd film, we exploited the thermal expansion mismatch between Pd and PDMS

during the sputtering process (**Figure 4a**). When the Pd film is sputtered onto PDMS, the PDMS thermally expands due to the energetic atoms and ions. As the temperature drops, the difference in the thermal expansion between Pd and PDMS results in biaxial compressive stress (σ_0) on the Pd film at temperature T, which is given by[35,36]

$$\sigma_0 = \frac{E_{Pd}\left(\alpha_{PDMS}^{T} - \alpha_{Pd}^{T}\right)\left(T_D - T\right)}{1 - \nu_{Pd}} \tag{3}$$

where α_{PDMS}^{T}, α_{Pd}^{T}, T_D and ν_{Pd} are the coefficient of thermal expansion of PDMS, the coefficient of thermal expansion of Pd, the deposition temperature and the Poisson's ratio of Pd, respectively.

Although it is difficult to control and measure the actual deposition temperatures on Pd/PDMS layers, the deposition temperature is more likely to increase with increasing sputtering time.[37] As a result, a thicker Pd film might exhibit stronger intrinsic stress under identical sputtering conditions. We fabricated test units with Pd films of different thicknesses. In this experiment, we used 1 cm × 1 cm Pd films formed without the patterning process to maintain the difference in the intrinsic stresses of the sputtered Pd films. We observed an increase in intrinsic compressive stress through the GISAXS pattern at the Pd/PDMS interface (Figure 4b, Note S4, Supporting Information). As the thickness of the Pd film increased, the highest scattering position gradually shifted to a relatively small q_z. This trend indicated that the out-of-plane tensile strain at the Pd/PDMS interface increased; therefore, this trend implicated that the increase in the in-plane compressive strain depended on the Pd thickness.

Figure 4c shows the capacitance change of the Pd thin films with thicknesses of 20, 30, 40 and 50 nm during the hydrogen absorption/desorption cycle (Figure S10, Supporting Information). The thicker Pd films displayed a higher maximum capacitance, indicating a smaller constraint strain. This observation aligns with the behavior observed for the patterned Pd discussed in the previous section (Figure 4d). This trend contrasted with the increase in intrinsic compressive in-plane strain. Notably, the change in the plateau pressure from the α phase to the β phase has a similar tendency to the increasing intrinsic compressive strain instead of the decreasing constraint strain while the desorption plateau pressures are similar for all Pd films (Figure 4e).

This observation indicates the qualitative difference between the influences of the constraint strain and intrinsic strain on the hydrogenation behavior of Pd. To elucidate this difference, we suggest that these two types of strain are involved in distinct stages of the phase transition reaction. Considering the magnitude of expansion induced by hydrogenation, the phase transition reaction from the α- to β-phase can be divided into two steps as follows:

$$Pd_{(\alpha)} + \frac{a}{2}H_2 \rightarrow PdH_{a_{(\alpha)}} \tag{4}$$

$$PdH_{a_{(\alpha)}} + \frac{b-a}{2}H_2 \rightarrow PdH_{b_{(\beta)}} \tag{5}$$

where a and b are the maximum hydrogen concentration in the α-phase and minimum hydrogen concentration in the β-phase, respectively. During the former reaction, the constraint-induced stress is minimal due to the low hydrogen concentration in the α-phase.[34] In this step, the mechanical constraint primarily arises

ADVANCED
SCIENCE NEWS
www.advancedsciencenews.com

ADVANCED
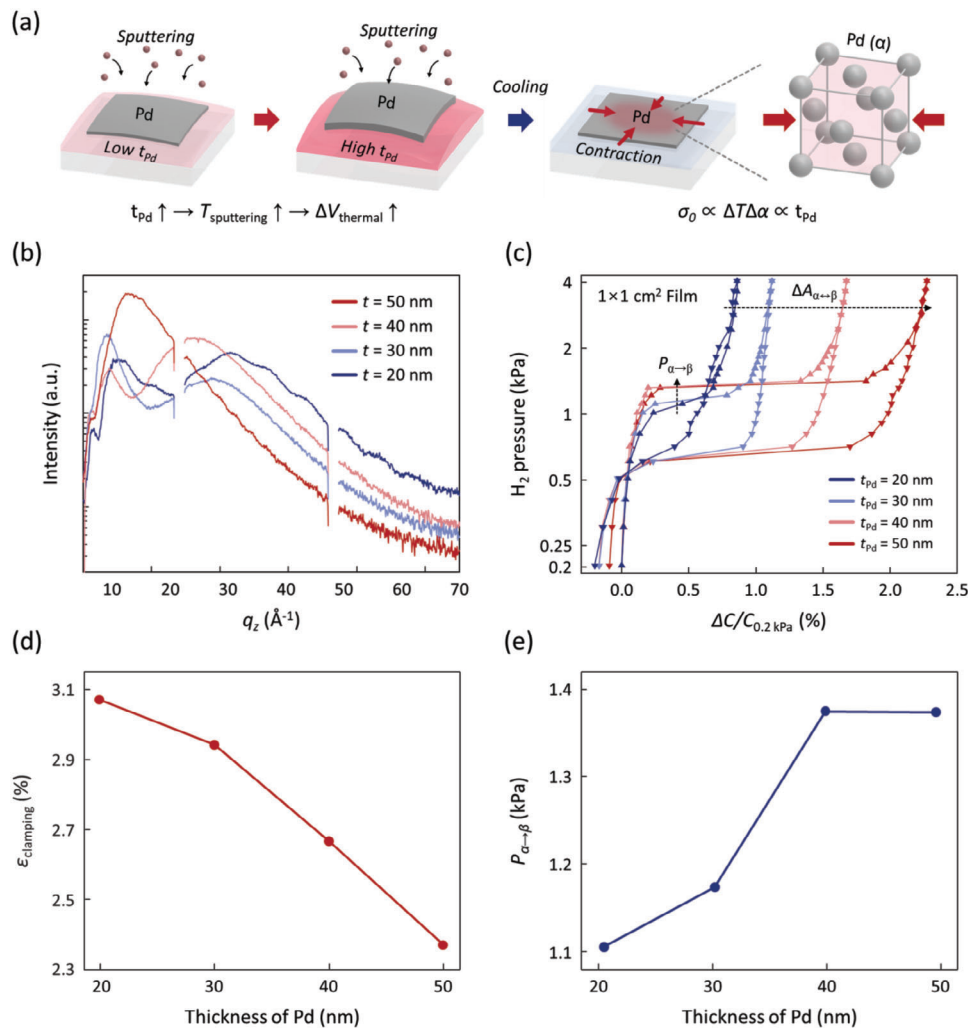**MATERIALS**
www.advmat.de

Figure 4. Effect of the initial stress on the Pd–H system. a) Schematic illustration of the thermally induced initial stress of the Pd film during the sputtering process onto the PDMS/Si substrate. b) 1D profiles extracted from GISAXS images along the out-of-plane in the initial state. c) Capacitance change of test units during the hydrogen ab- (▲)/desorption (▼) cycle for different thicknesses of the Pd film. d) Relative change in the interplanar distance (blue line) and constraint strain (red line) of Pd films with different thicknesses. The relative change in the interplanar distance was estimated from the average in the (111), (200), and (220)-directions. e) Plateau pressures from the α- to β-phase for different thicknesses of the Pd films.

from the strain imposed by the initial state, such as the intrinsic strain of Pd. In contrast, in the latter reaction, the constraint-induced stress becomes predominant due to the substantial volume expansion from the α- to β-phase.

According to the theory of open two-phase systems with a coherent interface,[15,38] the phase transition of an M–H system requires the excess free energy of the reactant phase to surpass the transformation-induced strain energy barrier. In other words, the thermodynamic barrier for the phase transition is determined by the chemical potential that allows the dissolution of hydrogen up to the maximum concentration of α-phase Pd in the reaction step (4). Subsequently, the transformation from the α- to β-phase should spontaneously occur, in which the hydrogen concentration of the product β-phase is determined by the chemical potential of the reactant α-phase. In this respect, the difference in the chemical potential of the interstitial hydrogen atom in Pd under

the initial stress $\sigma_{x,y,z}$ can be described as follows[39,40] (Note S3, Supporting Information):

$$\mu_H - \mu_H^{free} = -\frac{\overline{V_H}}{3}\left(\sigma_x + \sigma_y + \sigma_z\right) \tag{6}$$

where μ_H^{free} and $\overline{V_H}$ are the chemical potential of the unstressed state and the partial molar volume of hydrogen in Pd, respectively. Equation (6), which we hereafter call the initial stress model, considers the difference in work needed to add a hydrogen volume to stressed α-phase Pd. In contrast, the elastic constraint model considers the elastic strain energy of compressed β-phase PdH$_b$ during the transformation step.

The initial stress model can also explain the constant plateau pressure from the β- to α-phase, combined with the proposed constraint behavior in the previous section. During the phase
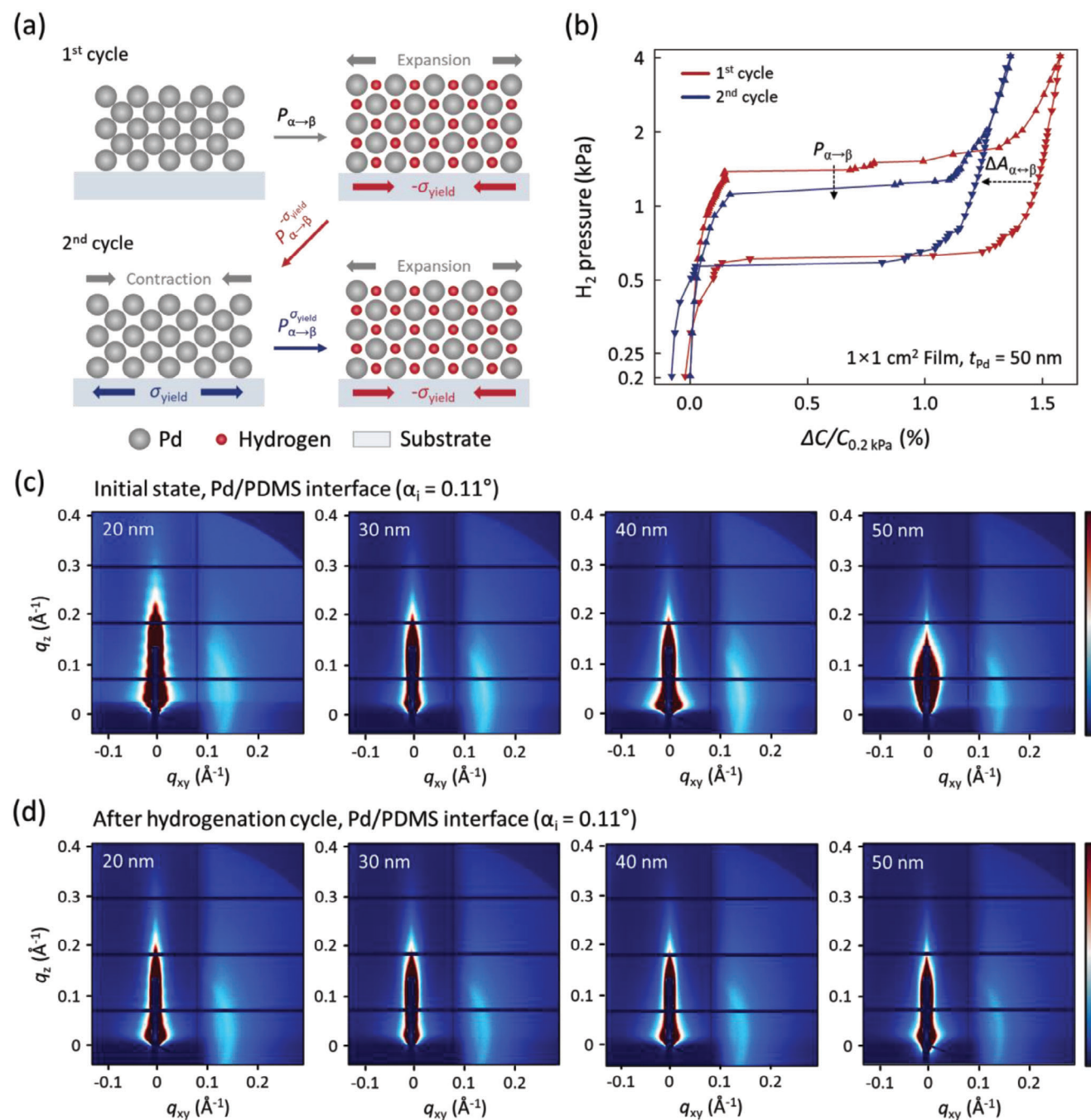
Figure 5. Cycling test. a) Schematic illustration of the change in the substrate-induced stress during repeated hydrogenation-induced expansion and contraction cycles. b) Capacitance change of the test units with the 50 nm-thick Pd film in the first and second hydrogen ab- (▲)/desorption (▼) cycles. c,d) GISAXS patterns for Pd films of various thicknesses in the initial state (c) and after the hydrogenation cycle (d).

transition from the α- to β-phase, the remaining in-plane initial stress of β-phase Pd should become equal to the yield strength regardless of the intrinsic stress in the α-phase due to plastic deformation. As a result, the differences in the intrinsic stress disappear, and the thermodynamic energy barriers for the phase transition from the β- to α-phase become similar.

To further validate the initial stress model, we conducted a cycling test. As shown in **Figure 5a**, after the hydrogen absorp-

tion/desorption cycle, an in-plane tensile stress is induced in the α-phase Pd film by the substrate constraint during volume contraction from the β phase to the α phase.[34,41] Similar deformation behavior during the hydrogen ab-/desorption cycle has been reported for the Nb–H system adhered to the substrate.[24,32] This in-plane tensile stress leads to a reduction in the plateau pressure from the α phase to the β phase and therefore induces hysteresis in the subsequent hydrogen absorption cycle. From the cycling

**ADVANCED
SCIENCE NEWS**

www.advancedsciencenews.com

**ADVANCED
MATERIALS**

www.advmat.de

test, we could observe the effect of initial stress with the same specimen while excluding the influence of different thicknesses associated with the deformation behaviour.[19]

Figure 5b illustrates the capacitance change of the test unit with the 50 nm-thick Pd film in the first and second hydrogen absorption/desorption cycles (Figure S11, Supporting Information). The maximum capacitance in the second cycle is smaller than that in the first cycle, which might be attributed to the in-plane expansion of α-phase Pd resulting from the initial tensile stress. In the second cycle, the decrease in the plateau pressure from the α- to β-phase was observed, which aligns with the prediction by the initial stress model.

While we cannot directly measure the in-plane tensile stress of the Pd film, the decrease in the plateau pressure of $\frac{P_{\alpha \to \beta}^{2\ cycle}}{P_{\alpha \to \beta}^{1\ cycle}}$ = 0.81 corresponds to a biaxial tensile stress of 460 MPa according to the initial stress model. This magnitude is consistent with previous research.[41] The similarity in XRD peak positions in the first and second cycles supports the assumption that the shift in the plateau pressure originates from the strain in the in-plane direction rather than that in the out-of-plane direction (Figure S12, Supporting Information)

The change in the initial stress of Pd after the hydrogenation cycle was experimentally confirmed by grazing-incidence small-angle X-ray scattering (GISAXS) measurements (Note S4, Supporting Information). Figure 5c,d show the GISAXS patterns of Pd films with different thicknesses before and after the hydrogenation cycle, respectively. In the measurements, the X-ray beam at an incident angle of α_i = 0.11° passed through the Pd/PDMS interface region, thereby demonstrating the influence of the constraint stress (detailed scattering information and GISAXS results in the bulk region are provided in Supporting Information). In the initial state before the hydrogenation cycle (Figure 5c), the GISAXS patterns present distinct variations in the thickness-dependent Pd crystal structure that arise from the effect of initial thermal stress during Pd deposition. However, after the hydrogenation cycle, similar scattering patterns can be observed in the GISAXS images (Figure 5d) regardless of the Pd thickness. This observation suggests that the discrepancies in the thermal stresses on the Pd films dissipate after the hydrogenation cycle. These results support that hydrogenation-induced plastic deformation can equalize the stress in Pd film regardless of the initial thermal stress.

3. Conclusion

We developed a capacitive-based system to monitor the hydrogenation/dehydrogenation process by measuring the areal expansion of an M–H system. Through this approach, we studied the influence of substrate constraint on the Pd–H system and found that if the excess constraint stress can be released by plastic deformation, the intensity of the substrate constraint minimally impacts the phase-transition pressure while the phase-transition pressure is sensitive to the magnitude of the initial stress. The thermodynamic influence of the substrate constraint can depend on the effectiveness of the suppression of the stress relaxation mechanism of the M–H system, such as plastic deformation, rather than on the constraint intensity itself. The constraint intensity itself can be useful for controlling the defor-

mation behavior during hydrogenation, including the magnitude of hydrogenation-induced expansion and plastic deformation, which in turn is related to the reversibility of the hydrogenation process. Our results provide insight into the role of substrate constraints under plastic deformation and demonstrate the potential of our capacitive-based measurement for investigating the mechanical–thermodynamic coupling of the M–H system.

4. Experimental Section

Preparation of Pd/PDMS/Si Test Units: A boron-doped silicon wafer with a 2000 Å-thick SiO_2 layer was chosen as the substrate. The wafer was cleaned through sonication with DI water, acetone, and IPA sequentially and dried with an N_2 gun. The PDMS base and curing agent (Sylgard 184, Dow Corning Corp.) were mixed at a weight ratio of 10:1 in a vial. Hexane (≥95%, Sigma Aldrich) was added to the PDMS mixture at a weight ratio of 3:1 and sonicated for 30 min. To enhance the adhesion between PDMS and the silicon wafer, the wafer was treated with O_2 plasma at 100 W for 3 min. The PDMS mixture was spin-coated onto the wafer at 3000 rpm for 30 s, followed by curing at 80 °C for 5 h on a hot plate. The wafer with the PDMS layer was cut into 2 × 2 cm^2 pieces, cleaned by sonication with acetone for 5 min and dried with an N_2 gun. A Pd thin film was deposited by using an ultrahigh vacuum direct current (UHV-DC) magnetron sputtering system (base pressure 7×10^{-8} Torr). A Pd thin film was deposited on the PDMS-coated wafer at a deposition rate of 3.52 Å s^{-1} and an Ar pressure of 1.2×10^{-4} Torr using a high-purity palladium target (99.99%).

To pattern the Pd thin film, the positive photoresist was spin-coated on the Pd thin film at 3000 rpm and soft baked at 60 °C on a hot plate for 10 min. The photoresist layer was exposed to UV for 15 s using a contact mask aligner and developed for 10 s, followed by rinsing with DI water. Then, the Pd thin film with the photoresist pattern was etched with 1 M $FeCl_3 \cdot 6H_2O$ solution (≥98%, Sigma Aldrich) for 5 min and rinsed with DI water. Finally, to remove the photoresist, the sample was immersed in acetone and rinsed with IPA. For the film-type samples fabricated without photolithography, a Pd thin film with a size of 1 × 1 cm^2 was deposited on the center of a 2 × 2 cm^2-sized wafer by masking with PI tape.

Measurement of the Capacitance Change upon Hydrogen Ab/Desorption: Before the measurement, Ag paste was applied on one side of the wavy Pd pattern and doped Si to make electrical contacts on the test unit. Capacitance measurement of the Pd/PDMS/Si capacitor in a gas chamber was carried out using a microprobe station system (MPS-PT, Nextron) equipped with an LCR Meter (E4980A, Agilent). The concentration of H_2 gas was controlled by mixing high-concentration H_2 gas (4%, >99.999%) and N_2 gas (>99.999%) at 1 atm using mass flow controllers.

Simulation: The finite element method (FEM) was used to analyze the hydrogenation-induced expansion of the Pd pattern on the PDMS/Si substrate. A static linear analysis under the isotropic expansion of Pd up to 3.5% was carried out by the open-source FEM software Code_Aster. In the simulation, the Young's moduli of Pd, PDMS and Si were 110 GPa, 2 MPa and 113 GPa, respectively. The Poisson's ratios of Pd, PDMS and Si were 0.39, 0.499 and 0.42, respectively. To simplify the simulation, the change in the mechanical properties of Pd upon hydrogenation was not considered.

X-Ray Diffraction Measurement: The XRD diffraction patterns of Pd films on PDMS/Si substrates were investigated with an X-ray diffractometer (SmartLab, Rigaku) using Cu Kα radiation. For the in situ XRD measurements, the Pd/PDMS/Si and Pd/SiO_2/Si test units were vacuum-sealed in a custom-made beryllium dome and then exposed to the intended hydrogen pressure.

Grazing-Incidence Small-Angle X-Ray Scattering (GISAXS) Measurement: GISAXS measurements were performed at the 3C SAXS-I beamline of the PLS-II synchrotron facility, Pohang Accelerator Laboratory (Pohang, Korea). The X-ray beam had photon energy of 10.24 keV (bandwidth d(λ)/λ of 1.5%), and the sample-to-detector distance was set to 2 m (confidence q range: 0.002 Å^{-1} < q < 0.286 Å^{-1}). The scattering angle was calibrated using a silver behenate standard. GISAXS data were acquired using an

Eiger4M detector and recorded with the X-ray beam at two different incident angles (0.11° and 0.056°) for an exposure time of ≈30 s. The GISAXS images were processed using PGIXS software.

Supporting Information

Supporting Information is available from the Wiley Online Library or from the author.

Acknowledgements

Conflict of Interest

The authors declare no conflict of interest.

Author contributions

W.L. supervised the research project. D.W.C. and Y.J.K developed the research concept, designed the experiments and analyzed the results. J.Y.P. designed the experiments and analyzed the results. G.K. conceived the research concept, designed the experiments, analyzed the results and wrote the first draft of the manuscript. S.L. designed and performed the experiments and analyzed the results. S.L. performed the experiments and analyzed the results. H.J.Y., H.C., Y.C., and T.-E.P. performed the experiments. K.H.L., W.S. and H.-S.L. discussed and commented on the results and the manuscript. All authors discussed the results and contributed to the writing of the manuscript.

Data Availability Statement

The data that support the findings of this study are available from the corresponding author upon reasonable request.

Keywords

[1] L. Schlapbach, A. Züttel, *Nature* **2001**, *414*, 353.
[2] H. Wang, H. J. Lin, W. T. Cai, L. Z. Ouyang, M. Zhu, *J. Alloys Compd.* **2016**, *658*, 280.
[3] W. Li, C. Li, H. Ma, J. Chen, *J. Am. Chem. Soc.* **2007**, *129*, 6710.
[4] M. Paskevicius, D. A. Sheppard, C. E. Buckley, *J. Am. Chem. Soc.* **2010**, *132*, 5077.
[5] R. Bardhan, L. O. Hedges, C. L. Pint, A. Javey, S. Whitelam, J. J. Urban, *Nat. Mater.* **2013**, *12*, 905.
[6] G. Liang, J. Huot, S. Boily, A. Van Neste, R. Schulz, *J. Alloys Compd.* **1999**, *292*, 247.
[7] W. Oelerich, T. Klassen, R. Bormann, *J. Alloys Compd.* **2001**, *315*, 237.
[8] L. Xie, Y. Liu, Y. T. Wang, J. Zheng, X. G. Li, *Acta Mater.* **2007**, *55*, 4585.
[9] J. J. Vajo, F. Mertens, C. C. Ahn, R. C. Bowman, B. Fultz, *J. Phys. Chem. B* **2004**, *108*, 13977.
[10] R. Gremaud, C. P. Broedersz, D. M. Borsa, A. Borgschulte, P. Mauron, H. Schreuders, J. H. Rector, B. Dam, R. Griessen, *Adv. Mater.* **2007**, *19*, 2813.
[11] H. Wang, H. Zhong, L. Ouyang, J. Liu, D. Sun, Q. Zhang, M. Zhu, *J. Phys. Chem. C* **2014**, *118*, 12087.
[12] P. Ngene, A. Longo, L. Mooij, W. Bras, B. Dam, *Nat. Commun.* **2017**, *8*, 1846.
[13] A. Baldi, M. Gonzalez-Silveira, V. Palmisano, B. Dam, R. Griessen, *Phys. Rev. Lett.* **2009**, *102*, 226102.
[14] A. Baldi, L. Mooij, V. Palmisano, H. Schreuders, G. Krishnan, B. J. Kooi, B. Dam, R. Griessen, *Phys. Rev. Lett.* **2018**, *121*, 255503.
[15] R. B. Schwarz, A. G. Khachaturyan, *Acta Mater.* **2006**, *54*, 313.
[16] R. Griessen, N. Strohfeldt, H. Giessen, *Nat. Mater.* **2016**, *15*, 311.
[17] A. Baldi, T. C. Narayan, A. L. Koh, J. A. Dionne, *Nat. Mater.* **2014**, *13*, 1143.
[18] A. Ulvestad, M. J. Welland, W. Cha, Y. Liu, J. W. Kim, R. Harder, E. Maxey, J. N. Clark, M. J. Highland, H. You, P. Zapol, S. O. Hruszkewycz, G. B. Stephenson, *Nat. Mater.* **2017**, *16*, 565.
[19] R. Gemma, P. Dobron, J. Cizek, A. Pundt, *Acta Mater.* **2014**, *67*, 308.
[20] S. Wagner, A. Pundt, *Int. J. Hydrogen Energy* **2016**, *41*, 2727.
[21] T. Yamamoto, H. Inui, M. Yamaguchi, *Intermetallics* **2001**, *9*, 987.
[22] C.-J. Chung, S.-C. Lee, J. R. Groves, E. N. Brower, R. Sinclair, B. M. Clemens, *Phys. Rev. Lett.* **2012**, *108*, 106102.
[23] J. A. Kammerer, X. Duan, F. Neubrech, R. R. Schröder, N. Liu, M. Pfannmöller, *Adv. Mater.* **2021**, *33*, 2008259.
[24] A. Pundt, U. Laudahn, U. V. Hülsen, U. Geyer, T. Wagner, M. Getzlafft, M. Bode, R. Wiesendanger, R. Kirchheim, *MRS Online Proc. Libr.* **1999**, *594*, 75.
[25] M. Hamm, V. Burlaka, S. Wagner, A. Pundt, *Appl. Phys. Lett.* **2015**, *106*, 243108.
[26] L. J. Bannenberg, F. A. A. Nugroho, H. Schreuders, B. Norder, T. T. Trinh, N.-J. Steinke, A. A. Van Well, C. Langhammer, B. Dam, *ACS Appl. Mater. Interfaces* **2019**, *11*, 15489.
[27] J.-Y. Sun, N. Lu, J. Yoon, K.-H. Oh, Z. Suo, J. J. Vlassak, *J. Mater. Res.* **2009**, *24*, 3338.
[28] S. Paik, G. Kim, S. Chang, S. Lee, D. Jin, K.-Y. Jeong, I. S. Lee, J. Lee, H. Moon, J. Lee, K. Chang, S. S. Choi, J. Moon, S. Jung, S. Kang, W. Lee, H.-J. Choi, H. Choi, H. J. Kim, J.-H. Lee, J. Cheon, M. Kim, J. Myoung, H.-G. Park, W. Shim, *Nat. Commun.* **2020**, *11*, 805.
[29] J. Lee, W. Shim, E. Lee, J.-S. Noh, W. Lee, *Angew. Chem., Int. Ed.* **2011**, *50*, 5301.
[30] H.-S. Lee, J. Kim, H. Moon, W. Lee, *Adv. Mater.* **2021**, *33*, 2005929.
[31] T. C. Merkel, V. I. Bondar, K. Nagai, B. D. Freeman, I. Pinnau, *J. Polym. Sci., Part B: Polym. Phys.* **2000**, *38*, 415.
[32] Y. Pivak, H. Schreuders, M. Slaman, R. Griessen, B. Dam, *Int. J. Hydrogen Energy* **2011**, *36*, 4056.
[33] A. Maeland, T. B. Flanagan, *J. Phys. Chem.* **1964**, *68*, 1419.
[34] S. Wagner, T. Kramer, H. Uchida, P. Dobron, J. Cizek, A. Pundt, *Acta Mater.* **2016**, *114*, 116.

[35] M. Ohring, *Materials Science of Thin Films: Depositon & Structure*, Academic Press, San Diego, CA **2001**.

[36] N. Bowden, S. Brittain, A. G. Evans, J. W. Hutchinson, G. M. Whitesides, *Nature* **1998**, *393*, 146.

[37] L. R. Shaginyan, J. G. Han, V. R. Shaginyan, J. Musil, *J. Vac. Sci. Technol. A* **2006**, *24*, 1083.

[38] R. B. Schwarz, A. G. Khachaturyan, *Phys. Rev. Lett.* **1995**, *74*, 2523.

[39] J. C. M. Li, R. A. Oriani, L. S. Darken, *Z. Für Phys. Chem.* **1966**, *49*, 271.

[40] H. A. Wriedt, R. A. Oriani, *Acta Metall.* **1970**, *18*, 753.

[41] N. Verma, R. Delhez, N. M. Van Der Pers, F. D. Tichelaar, A. J. Böttger, *Int. J. Hydrogen Energy* **2021**, *46*, 4137.